Supplementary Online Materials

I. CALCULATION OF WINDING NUMBERS

We first illustrate the appearance of two winding numbers, Eqs. (8)–(11) in the main text, from the properties of the complex effective "magnetic field" $\mathbf{B}$, Eq. (1). This field lies in the (x, y)-plane, and can be characterized by its *magnitude* and azimuthal *direction* angle: $\mathbf{B} = B(\cos\phi, \sin\phi, 0)$.

First, the complex direction angle is given by

$$\phi = \arctan\left(\frac{B_y}{B_x}\right) = \arctan\left(\frac{m}{k_x - isk_y}\right). \quad (S1)$$

The distribution of its real part, $\mathrm{Re}\,\phi(\mathbf{k})$, is shown in Fig. S1(a). Integrating its k_x-gradient along the contour shown in Fig. S1(a) yields the first winding number $w_1(k_y)$, Eqs. (8) and (9), shown in Fig. S1(c). Note that only smooth gradients of $\mathrm{Re}\,\phi(k_x)$ contribute to the integral, but not π jumps. Furthermore, the imaginary part of the angle ϕ does not contribute to the integrals (8) and (9). Therefore, the winding number w_1 is an extention of the Hermitian winding number based on the Berry phase and direction of the $\mathbf{B}$-field [1, 2].

Second, the magnitude of the $\mathbf{B}$-field is also *complex* in the non-Hermitian case. It is equal to the eigenvalue λ^+:

$$B = \sqrt{B_x^2 + B_y^2} = \sqrt{(k_x - isk_y)^2 + m^2} = \lambda^+. \quad (S2)$$

The complex character of this quantity is characterized by its phase $\mathrm{Arg}\,\lambda^+$. The distribution $\mathrm{Arg}\,\lambda^+(\mathbf{k})$ is depicted in Fig. S1(b). Integrating its k_x-gradient along the same contour yields the second winding number $w_2(k_y)$, Eqs. (10) and (11), shown in Fig. S1(d). Since the nontrivial phase behavior of eigenvalues is a purely non-Hermitian feature, the w_2 number characterizes "non-Hermitian" and "mixed" anomalous edge modes [3, 4].

Importatly, the above description of the winding numbers, based on the properties of the complex $\mathbf{B}$-field, is universal and can be applied to other non-Hermitian two-level systems. Below we show this for two examples of 2D lattice systems.

II. TIGHT-BINDING MODELS

One important distinction between the continuum model studied in the main text and lattice models is the periodic boundary conditions imposed by the 2D Brillouin zone in the latter. To satisfy periodic boundary conditions, any branch cut in the eigenvalues must terminate at an inequivalent EP, such that $\sum q_2 = 0$. Therefore, regularizing Eq. (1) of the main text to a lattice
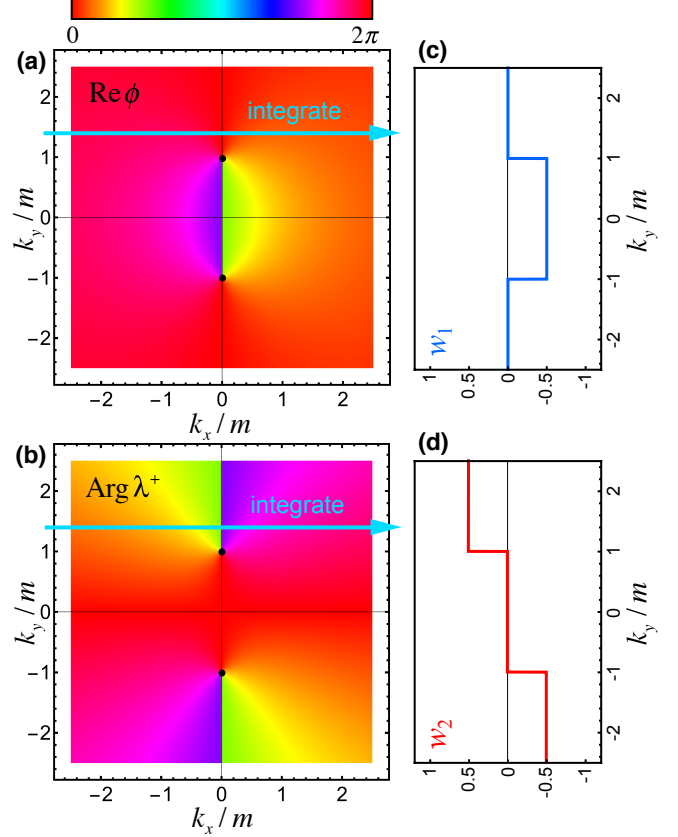

FIG. S1: Color-coded $\mathbf{k}$-distributions of (a) the real part of the azimuthal angle ϕ of the $\mathbf{B}$-field and (b) the phase of the complex field magnitude $B = \lambda^+$. Black dots indicate the EPs. Integration of the k_x-gradients of these angles along the k_y-dependent cyan contour yields the two winding numbers $w_1(k_y)$ and $w_2(k_y)$, Eqs. (8)–(11), shown in panels (c) and (d).

will double the EP pairs, with the partners having opposite charges. This is analogous to the doubling of Dirac points in graphene-like systems implied by the Nielsen-Ninomiya theorem. Nevertheless, for most orientations of a lattice edge or domain wall, the doubled partners are decoupled. Nonzero winding numbers and edge modes will still occur within the finite range of momenta between the doubled partners [5].

Here we show how to achieve fractional winding numbers in ring resonator lattices. We consider anisotropic honeycomb lattices with inter-resonator coupling mediated by nonresonant link rings. In the Hermitian limit, the honeycomb lattice hosts Dirac point degeneracies characterized by integer winding numbers. Introducing non-Hermitian couplings by inserting gain or loss into the link rings splits the Dirac points into pairs of EPs, generating fractional winding numbers. We will consider two

types of non-Hermitian couplings: balanced gain and loss within each link ring, which is described by a real asymmetric Hamiltonian [6], and link rings with pure gain or loss, generating a complex symmetric Hamiltonian [7]. These two cases result in different trajectories of the EPs in momentum space as a function of the non-Hermiticity strength γ.

A. Model 1

We begin by considering a non-Hermitian coupling generated by inserting balanced gain and loss into one of the three link rings, shown in Fig. S2. For the clockwise-circulating resonator modes, intracell hopping from the "A" sublattice to the "B" sublattice occurs via the lossy half of the link resonator. Conversely, hopping from "B" to "A" occurs through the half of the link resonator with gain. The corresponding Bloch Hamiltonian is asymmetric [6],

$$\hat{H} = \begin{pmatrix} 0 & ce^{-\gamma} + e^{-i\mathbf{k}\cdot\mathbf{a}_1} + e^{-i\mathbf{k}\cdot\mathbf{a}_2} \\ ce^{\gamma} + e^{i\mathbf{k}\cdot\mathbf{a}_1} + e^{i\mathbf{k}\cdot\mathbf{a}_2} & 0 \end{pmatrix},$$
(S3)

where c is the intracell coupling strength, γ is the strength of the gain and loss, and the other two Hermitian couplings have been normalized to 1. Here, $\mathbf{k}$ is the Bloch wavevector and the lattice vectors are $\mathbf{a}_1 = \frac{a}{2}(1, \sqrt{3})$, $\mathbf{a}_2 = \frac{a}{2}(-1, \sqrt{3})$, $\mathbf{a}_3 = a(1,0) = \mathbf{a}_1 - \mathbf{a}_2$, where a is the lattice period.

Note that the Hamiltonian (S3) has a chiral symmetry: $\{\hat{H}, \hat{\sigma}_z\} = 0$. For the bulk-edge correspondence to hold in a lattice, parity-time ($\mathcal{PT}$) symmetry was also required in [4]. Here $\mathcal{P} = (y \to -y) \bigotimes \hat{\sigma}_x$ is the reflection $y \to -y$ (which swaps the two sulattices), and $\mathcal{T} = \hat{\sigma}_y K$, where K is complex conjugation. The operator $\mathcal{T}$ takes a nontrivial form because Eq. (S3) is written in the basis of circulating modes, which is not $\mathcal{T}$-symmetric [3].

Akin to Eq. (1), the Hamiltonian (S3) can be parametrized as $\hat{H} = \mathbf{B} \cdot \hat{\boldsymbol{\sigma}}$ (using non-permuted Pauli matrices) with the two-component complex **B**-field:

$$B_x = c\cosh\gamma + 2\cos\left(\frac{k_x a}{2}\right)\cos\left(\frac{\sqrt{3}k_y a}{2}\right),$$

$$B_y = -ic\sinh\gamma + 2\cos\left(\frac{k_x a}{2}\right)\sin\left(\frac{\sqrt{3}k_y a}{2}\right). \quad (S4)$$

Notably, if k_x is taken as a fixed parameter, this model becomes equivalent to the 1D model studied in Ref. [4].

In the Hermitian limit $\gamma = 0$, the isotropic ($c = 1$) lattice hosts Dirac points (Hermitian degeneracies) at the **K** points, $\mathbf{K}_\pm = \frac{2\pi}{3a}(\pm 1, \sqrt{3})$. Reciprocal lattice vectors $\mathbf{G}_1 = \frac{2\pi}{a}(1, \frac{1}{\sqrt{3}})$, $\mathbf{G}_2 = \frac{2\pi}{a}(-1, \frac{1}{\sqrt{3}})$, $\mathbf{G}_3 = \frac{2\pi}{a}(1,0)$ relate equivalent **K** points. The anisotropy $c \neq 1$ shifts the Dirac points along the k_x axis (i.e. in the $\mathbf{G}_3$ direction)
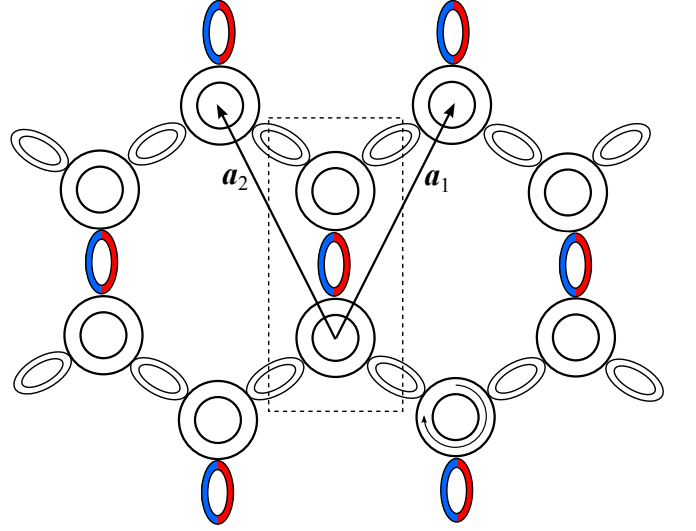

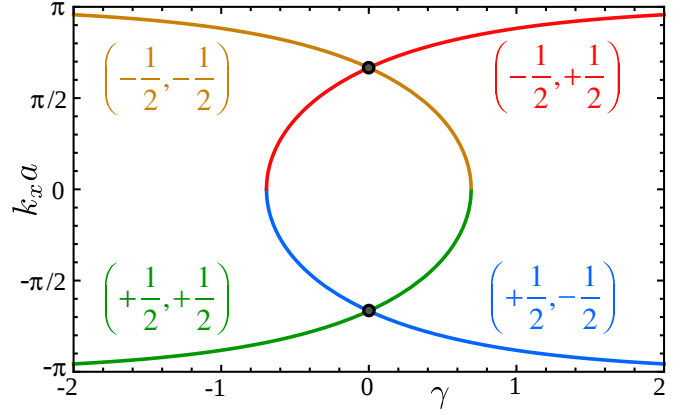FIG. S2: Honeycomb lattice formed by ring resonators with gain/loss (red/blue) in one of the three link rings.

FIG. S3: Positions of exceptional points with charges (q_1, q_2) as a function of the non-Hermitian parameter γ. Black points indicate the Dirac points in the Hermitian limit $\gamma = 0$.

towards their partners. They merge and annihilate at the critical points $c = 0, 2$. A nonzero γ splits each Dirac point into a pair of EPs with charges (q_1, q_2) and k_x-positions

$$\left(+\frac{1}{2}, -\frac{1}{2}\right), \quad k_x = -2\sec^{-1}\left(\frac{2e^\gamma}{c}\right),$$

$$\left(-\frac{1}{2}, +\frac{1}{2}\right), \quad k_x = 2\sec^{-1}\left(\frac{2e^\gamma}{c}\right),$$

$$\left(+\frac{1}{2}, +\frac{1}{2}\right), \quad k_x = -2\cos^{-1}\left(\frac{ce^\gamma}{2}\right),$$

$$\left(-\frac{1}{2}, -\frac{1}{2}\right), \quad k_x = 2\cos^{-1}\left(\frac{ce^\gamma}{2}\right). \quad (S5)$$

Figure S3 plots the EP positions as a function of γ (assuming $c = 1$). Note the vanishing total charge when EPs coalesce and annihilate at $\gamma = \pm \ln\frac{c}{2}$. On the other hand,
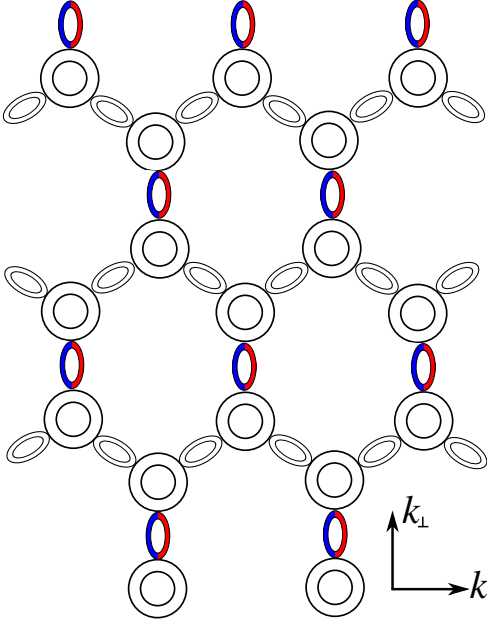
FIG. S4: Honeycomb lattice with "bearded" edge.

when EPs coalesce to form Dirac points, $\sum q_1 = \pm 1$ and $\sum q_2 = 0$. By tuning (c, γ) one can control the relative positions and number of EPs in the bulk Hamiltonian. Note that the $m = 0$ limit of our continuum Hamiltonian (1) (coalescence of EPs with $\sum q_2 \neq 0$) is not realized in this model.

We now consider a lattice with "bearded" edges shown in Fig. S4. This edge termination respects both the chiral and $\mathcal{PT}$ symmetries. To determine the resulting edge states, one must project $\boldsymbol{k} = k_{\parallel} \boldsymbol{e}_{\parallel} + k_{\perp} \boldsymbol{e}_{\perp}$ onto components parallel and perpendicular to the boundary, described by the reciprocal space basis vectors $\boldsymbol{e}_j = \boldsymbol{\Gamma}_j / |\boldsymbol{\Gamma}_j|$, with $\boldsymbol{\Gamma}_{\parallel} = \frac{2\pi}{a}(1,0)$ and $\boldsymbol{\Gamma}_{\perp} = \frac{4\pi}{a\sqrt{3}}(0,1)$ [5]. $k_{\parallel} \in \frac{\pi}{a}[-1,1]$ becomes a parameter and the winding numbers of each domain are calculated over the 1D Brillouin zone defined by $k_{\perp} \in \frac{2\pi}{a\sqrt{3}}(-1,1)$ using Eqs. (8) and (10) for the field (S4) (see also Section I above).

Figure S5 shows $\boldsymbol{k}$-distributions of the direction angle $\mathrm{Re}\,\phi$ and the phase $\mathrm{Arg}\,B$ of the $\boldsymbol{B}$-field (S4), as well as the corresponding winding numbers $w_1(k_{\parallel})$ and $w_2(k_{\parallel})$ for $\gamma = 0.4$. One can see that tuning $k_{\parallel}$ through the EPs changes the winding numbers by $\pm \frac{1}{2}$. Furthermore, there are $k_{\parallel}$-intervals with $w_1 = 0, \frac{1}{2}, 1$ and $w_2 = 0, -\frac{1}{2}\mathrm{sgn}(\gamma)$. Therefore "bearded" edges or domain walls between regions with different $\gamma_1 \neq \gamma_2$ can host the non-Hermitian edge modes discussed in the main text.

To verify the existence of the predicted edge states, we numerically diagonalized $\hat{H}$ on a semi-infinite strip with bearded edges. For sufficiently small k_x both edges support localized modes and they have opposite chiralities. Increasing k_x, one of the edge states becomes more

strongly localized, while the other becomes more weakly localized, disappearing when the EP is crossed and $w_{1,2}$ become fractional. The sole remaining edge state is defective, i.e. there are two zero energy eigenvalues sharing the same eigenvector.

This model also provides a simple way to understand the emergence of the anomalous edge states. For $\gamma > 0$, hopping in the $+y$ direction is accompanied by amplification which will counteract the evanescent decay of a state localized to the lower edge, which delocalizes when the amplification rate exceeds the evanescent decay rate and ceases to exist. In contrast, hopping in the $-y$ direction is accompanied by attenuation, which enhances the localization of the zero-energy states at the upper edge.
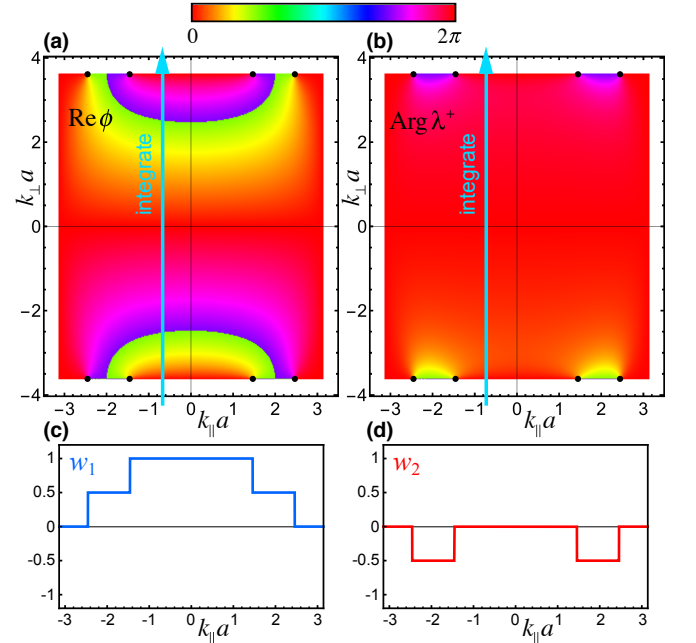

FIG. S5: Color-coded $\boldsymbol{k}$-distributions of (a) the direction $\mathrm{Re}\,\phi$ (b) the phase $\mathrm{Arg}\,B = \mathrm{Arg}\,\lambda^+$ of the complex $\boldsymbol{B}$-field (S4). Black dots indicate the EPs. Integration of the $k_{\perp}$-gradients of these angles along the $k_{\parallel}$-dependent cyan contour yields the two winding numbers $w_1(k_y)$ and $w_2(k_y)$, Eqs. (8) and (10), shown in panels (c) and (d). Here parameters are $c = 1$ and $\gamma = 0.4$.

B. Model 2

To realize a lattice counterpart of our continuum Hamiltonian Eq. (1), we require a non-Hermitian term that is asymmetric in k. This can be achieved if a pair of links are given balanced gain and loss, as shown in Fig. S6 and described by the Bloch Hamiltonian

$$\hat{H} = \begin{pmatrix} 0 & c + (1 - i\gamma)e^{-i\boldsymbol{k}\cdot\boldsymbol{a}_1} + (1 + i\gamma)e^{-i\boldsymbol{k}\cdot\boldsymbol{a}_2} \\ c + (1 - i\gamma)e^{i\boldsymbol{k}\cdot\boldsymbol{a}_1} + (1 + i\gamma)e^{i\boldsymbol{k}\cdot\boldsymbol{a}_2} & 0 \end{pmatrix}. \tag{S6}$$

Here, γ is the dissipative coupling strength describing the gain/attenuation imposed by passing through one of the link resonators [7]. This model shares the same chiral and $\mathcal{PT}$ symmetries as Eq. (S3), but now the non-Hermitian term (the imaginary part of the effective $\mathbf{B}$-field) is asymmetric in k_x:

$$B_x = c + 2\cos\left(\frac{k_x a}{2}\right)\cos\left(\frac{\sqrt{3}k_y a}{2}\right) + 2i\gamma\sin\left(\frac{k_x a}{2}\right)\sin\left(\frac{\sqrt{3}k_y a}{2}\right),$$

$$B_y = 2\cos\left(\frac{k_x a}{2}\right)\sin\left(\frac{\sqrt{3}k_y a}{2}\right) - 2i\gamma\sin\left(\frac{k_x a}{2}\right)\cos\left(\frac{\sqrt{3}k_y a}{2}\right). \tag{S7}$$

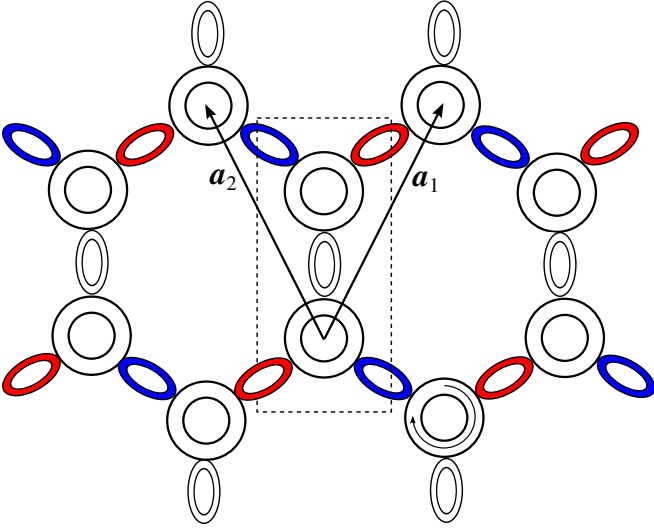
FIG. S6: Honeycomb lattice formed by ring resonators with dissipative coupling (gain/loss in two of the three link rings).

FIG. S7: Positions of exceptional points with charges (q_1, q_2) as a function of the non-Hermitian parameter γ. Solid lines indicate the EPs at the Brillouin zone edge ($k_y = 2\pi/\sqrt{3}$), while dashed lines correspond to the zone centre $k_y = 0$. Black points indicate the Dirac points in the Hermitian limit $\gamma = 0$.

Similarly to above, a small γ splits the Dirac points confined to the line $k_y a = 2\pi/\sqrt{3}$ into a pair of EPs with positions k_x plotted in Fig. S7. However, increasing γ now leads to the coalescence of an EP pair with the same non-Hermitian charge q_2 at the Brillouin zone edge $k_x a = \pm\pi$. Since their total charge is nonzero they cannot annihilate; instead they enter the second Brillouin zone $|k_x a| > \pi$, which is equivalent to the line $k_y = 0$ in the first Brillouin zone (dashed lines in Fig. S7). Meanwhile, the second pair of EPs which approaches $k_x = 0$ reproduces the continuum Hamiltonian Eq. (1): Expanding $\boldsymbol{k} = (0, \frac{2\pi}{\sqrt{3}a}) + \boldsymbol{p}$ we obtain, to first order in the displacement $\boldsymbol{p}$, the effective $\mathbf{B}$-field components $B_x \simeq c - 2$ (a mass term) and $B_y \simeq i\gamma p_x a + \sqrt{3}p_y a$ (an anisotropic momentum term).

Similarly to the previous examples, in Fig. S8 we plot the $\text{Re}\,\phi(\mathbf{k})$ and $\text{Arg}\,\lambda^+(\mathbf{k})$ distributions, together with the corresponding winding numbers $w_1(k_\parallel)$ and $w_2(k_\parallel)$, for the Hamiltonian (S6) and $\mathbf{B}$-field (S7). The resulting
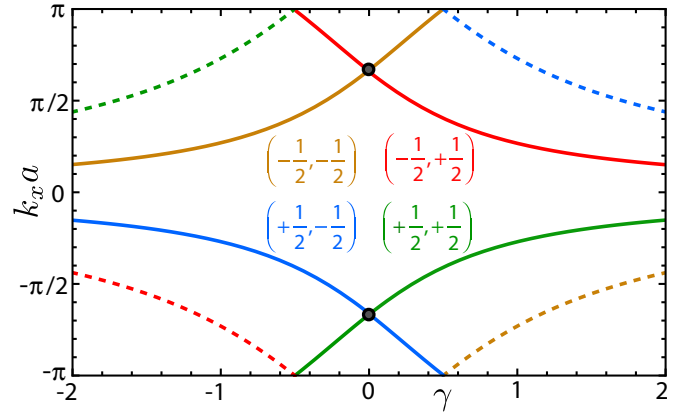
winding number for a bearded edge w_1 (w_2) is symmetric (antisymmetric) in $k_\parallel$, which provides a tight-binding-model analogue of Eqs. (9) and (11) and Fig. (S1).

Finally, let us remark on the key difference between the two lattice models considered here and previously-studied models of honeycomb lattices with $\mathcal{PT}$ symmetry based on a non-Hermitian sublattice potential $B_z = i\gamma\hat{\sigma}_z \neq 0$ [8]. In addition to reflection symmetry $\mathcal{P}$, two-dimensional lattices can have rotational symmetry $\mathcal{R}$. In this case (occurring in Ref. [8]), the Bloch Hamiltonian $\hat{H}(\boldsymbol{k})$ has a $\mathcal{PT}$ symmetry at *every* wavevector $\boldsymbol{k}$ and the energy eigenvalues are always purely real or imaginary. This constraint prevents the appearance of isolated exceptional points, which require complex eigenvalues, and instead results in the splitting of Hermitian Dirac points into ring degeneracies, which are unstable under further perturbations that break the $\mathcal{PT}$ symmetry. In contrast, in our models Eq. (S3) and Eq. (S6) the $\mathcal{PT}$ symmetry relates the Bloch Hamiltonians at inequivalent momenta
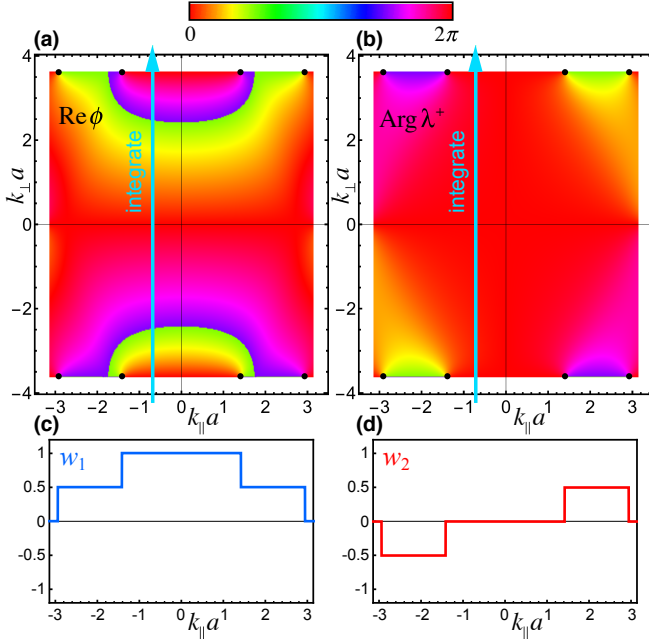
FIG. S8: Same as in Fig. S5 but for the tight-binding model 2 with the Hamiltonian (S6) and **B**-field (S7). Parameters are $c = 1$ and $\gamma = 0.4$.

$\hat{H}(k_x, k_y)$ and $\hat{H}(-k_x, k_y)$. Therefore the Bloch wave spectrum is in general complex, allowing the appearance of isolated non-Hermitian degeneracies (that are stable against small perturbations) and nonzero winding numbers w_2.

III. COUNTING ZERO MODES WITH THE INDEX THEOREM

Given a non-Hermitian Hamiltonian $\hat{H}$, we can define the Hermitian Hamiltonian

$$\hat{\mathcal{H}} = \hat{H}^\dagger \hat{H}. \qquad (S8)$$

If $\hat{H}|\psi\rangle = 0$, then $\hat{\mathcal{H}}|\psi\rangle = 0$. Conversely, if $\hat{\mathcal{H}}|\psi\rangle = 0$, then $\langle\psi|\hat{H}^\dagger\hat{H}|\psi\rangle = 0$, which implies that $\hat{H}|\psi\rangle = 0$. Note that this holds for any choice of inner product, and does not rely on the eigenvectors of $\hat{H}$ being orthogonal (they generally are not). Using the non-Hermitian Hamiltonian $\hat{H}$ from Eq. (5), we obtain

$$\hat{\mathcal{H}} = (p_x - \hat{\sigma}_y s A_x)^2 + (s p_y - \hat{\sigma}_y A_y)^2 + \hat{\sigma}_y B(x,y) \quad (S9)$$

where $p_i = -i\partial_i$, $\mathbf{A} = (s\text{Im}(m), \text{Re}(m))$, and $B(x,y) = \partial_x A_y - \partial_y A_x$.

Let us project to the eigenspace of $\hat{\sigma}_y$, thus replacing $\hat{\sigma}_y$ with $\sigma = \pm 1$. Now the zero modes of $\hat{\mathcal{H}}$ can be counted via a procedure originally introduced by Aharonov and Casher [9]. Define the canonical momentum operators

$$\pi_x = p_x - s\sigma A_x \; ; \; \pi_y = s p_y - \sigma A_y, \qquad (S10)$$

which obey the commutation relations $[\pi_x, \pi_y] = i\sigma B$. The Hermitian Hamiltonian $\hat{\mathcal{H}}$ can then be written as

$$\hat{\mathcal{H}} = (\pi_x + i\pi_y)(\pi_x - i\pi_y). \qquad (S11)$$

As we have argued above, a zero mode $|\psi\rangle$ must satisfy $(\pi_x - i\pi_y)|\psi\rangle = 0$. In terms of the wavefunction,

$$(-i\partial_x - s\partial_y - s\sigma A_x + i\sigma A_y)\psi(x,y) = 0. \qquad (S12)$$

Assuming $\nabla \cdot \boldsymbol{A} = 0$, we can let

$$A_x = \partial_y \varphi \; , \; A_y = -\partial_x \varphi. \qquad (S13)$$

With this gauge choice, the magnetic field is the source of a potential φ:

$$\nabla^2 \varphi(x,y) = B(x,y). \qquad (S14)$$

We substitute this back into Eq. (S12), and make the further gauge substitution

$$\psi(x,y) = \exp[-\sigma\varphi(x,y)]f(x,y). \qquad (S15)$$

Then $f(x,y)$ obeys

$$(\partial_x - is\partial_y)f(x,y) = 0. \qquad (S16)$$

In the first case of interest, $s_1 = s_2 = 1$, $f(x,y)$ is analytic in the complex plane, and hence cannot be normalized. Thus, the normalization of ψ must arise from the exponential factor in Eq. (S15). Using Eq. (S14), we write

$$\varphi(r) = \int dr' G(r - r')B(r'), \qquad (S17)$$

$$G(r - r') = \frac{1}{2\pi} \ln\left(\frac{|r - r'|}{l_B}\right). \qquad (S18)$$

Here, l_B is the magnetic length that serves as the cut-off of the theory. For $r \gg r'$,

$$\varphi(r) \to \ln\left(\frac{r}{l_B}\right)^{\Phi/2\pi}, \qquad (S19)$$

where

$$\Phi = \iint dx\, dy\, (\partial_x A_y - \partial_y A_x) = 2\pi(N + \epsilon). \qquad (S20)$$

Here, N is an integer and $0 < \epsilon < 1$. Substituting this back into Eq. (S15), we arrive at

$$\psi(x,y) = \left(\frac{r}{l_B}\right)^{-\sigma\Phi/2\pi} f(x,y). \qquad (S21)$$

Next, we can expand the analytic function $f(x,y)$ with

$$f(x,y) = f(z) = z^j, \qquad (S22)$$

where $z = x + iy$. The resulting wave function is

$$\psi_j(z) = \left(\frac{|z|}{l_B}\right)^{-\sigma\Phi/2\pi} z^j. \qquad (S23)$$

For $\sigma\Phi > 0$, we require $j = 0, 1, 2, \ldots, N-1$, so that $\psi_j(z)$ is normalizable. For $\sigma\Phi < 0$, however, there are no normalizable zero modes. Thus, $\hat{\mathcal{H}}$ has a total of N zero modes. The zero modes are polarized either spin-up ($\sigma = +1$) or spin-down ($\sigma = -1$), depending on the sign of the total magnetic flux Φ. The flux Φ is determined by the mass profile $m(x,y) = m(z)$, which must be a complex analytic function according to Eq. (S13).

In the second case, $s_1 = -s_2 = s$, $f(x,y) = f(z)$ is a piecewise-analytic function which can be decomposed in medium 1 using the Cauchy integral formula as

$$f(z) = \frac{1}{2\pi i} \oint \frac{f(t)}{t - z} dt, \qquad (S24)$$

where the integral is over the boundary between the two media. The analytic function $f^*(z)$ in medium 2 can be obtained similarly by requiring the continuity of ψ at the interface. Since $f(z)$ is now normalizable, zero modes can exist even when the flux Φ vanishes, in which case they will be spin-degenerate. A nonzero flux Φ will generate an imbalance between the number of spin-up and spin-down modes.

Suppose now that $m = m(x)$ forms a straight domain wall in the vicinity of $x = 0$ with mass parameters $m_{1,2}$ in the limit $|x| \to \infty$. A straightforward calculation shows that $\varphi(x) \to -m_1 x$, $\varphi(x \to \infty) = -m_2 x$,

the magnetic flux per unit length is $(m_2 - m_1)$, and $f(x,y) \propto \exp(-s_{1,2}kx + iky)$. The resulting wavefunction is

$$\psi(x,y) \sim \exp\left[iky - s_{1,2}kx - \sigma\varphi(x)\right], \qquad (S25)$$

reproducing the conditions for normalizable zero modes, Eqs. (7), discussed in the main text.

[1] M. S. Rudner and L. S. Levitov, Phys. Rev. Lett. **102**, 065703 (2009).
[2] K. Esaki, M. Sato, K. Hasebe, and M. Kohmoto, Phys. Rev. B **84**, 205128 (2011).
[3] H. Schomerus, Opt. Lett. **38**, 1912 (2013); S. Malzard, C. Poli, and H. Schomerus, Phys. Rev. Lett. **115**, 200402 (2015).
[4] T.E. Lee, Phys. Rev. Lett. **116**, 133903 (2016).
[5] P. Delplace, D. Ullmo, and G. Montambaux, Phys. Rev. B **84**, 195452 (2011).
[6] S. Longhi, D. Gatti, G. Della Valle, Phys. Rev. B **92**, 094204 (2015).
[7] S. Longhi, Phys. Rev. A **93**, 022102 (2016).
[8] A. Szameit, M. C. Rechtsman, O. Bahat-Treidel, and M. Segev, Phys. Rev. A **84**, 021806(R) (2011); H. Ramezani, T. Kottos, V. Kovanis, and D. N. Christodoulides, Phys. Rev. A **85**, 013818 (2012); F. Bagarello and N. Hatano, Proc. R. Soc. A **472**, 0365 (2016).
[9] Y. Aharonov and A. Casher, Phys. Rev. A **19**, 2461 (1979).